Observation of an excess of di-charmonium events in the four-muon final state with the ATLAS detector

Alina Isobel Hagan[a] for the ATLAS Collaboration

[a]*Lancaster University,*
Bailrigg, Lancaster, UK

E-mail: alina.hagan@cern.ch

An exploration of the $4mu$, di-charmonium channel in search for a full-charm tetraquark of the form $cc\bar{c}\bar{c}$ is conducted using the ATLAS detector with 140 fb^{-1} of pp data at $\sqrt{s}$ = 13 TeV. Both the di-J/ψ and the $J/\psi + \psi(2S)$ channels are explored and excesses over the background corresponding to a resonance at 6.9 GeV are seen with statistical significance of > 5 σ and 4.7 σ, respectively. At lower mass ranges, a broader structure can be observed, though its nature cannot be discerned with current data.

1. Introduction

Alongside the existence of mesons and baryons, tetraquark and pentaquark states can also exist under the constrains of color confinement. The first experimental evidence for a candidate of these exotic states was recorded by the Belle Collaboration in 2003 [1], the $X(3872)$. This has been the advent of a new 'particle zoo', an evolution of hadron spectroscopy. Fast forwarding to 2020, LHCb [2] saw a narrow structure in the di-$J/\psi(4\mu)$ channel at 6.9 GeV. It is possible to interpret this state, $X(6900)$, as a full-charm tetraquark, $T_{cc\bar{c}\bar{c}}$ [3].

Along with the 6.9 GeV occurrance, LHCb also sees an enhancement in the mass spectrum closer to the di-J/ψ threshold. The excess associated with $X(6900)$ is also above the $J/\psi + \psi(2S)$ threshold, so this could be observed this in both channels. ATLAS explores both the di-J/ψ and $J/\psi + \psi(2S)$ channels, in a differing phase space region to LHCb. This study uses 140 fb^{-1} and a 4μ final state.

2. The ATLAS Detector

The ATLAS experiment is a general purpose detector with a forward-backwards cylindrical geometrey and nearly complete 4πsr coverage in solid angle. Its construction consists of four main components; starting from the innermost ther is the Inner Detector (ID), layered silicon pixel and microstrip technologies and a transition radiation tracker. This is immersed in a 2 T axial magnetic field, provided by the Central Solenoidal Magnet CSM. Next radially is the LAr calorimiter for high resolution EM energy measurements of electrons and photons. Then the hadronic calorimeter, of steel/scintillator-tile construction. Finally, the Muon Spectrometer systems are on the outer layer. These systems are linked together by the ATLAS Trigger and Data Aquisition system (TDAQ), which controls the detector readout.

3. Samples and Background Estimation

Expectations of signal and background processes, yield and shape, are derived from Monte Carlo (MC) and data-driven estimates. Multiple background sources are used; di-J/ψ contribution from both SPS and DPS processes, non-prompt contributions of J/ψ from b decays and the contribution from uncorrelated prompt J/ψ combined with non-resonant $\mu\mu$ pairs, respectively. $J/\psi + \psi(2S)$ feed-down is included in and is modelled in the di-jpsi channel. A pileup reweighting is performed to match MC pp interactions per crossing to that of the data. For MC there are no interferences assumed to occur between the resonances, for each resonance, assume a 100 MeV width. All events are reconstucted with ATLAS offline software, and the data selection is provided by using a trigger requiring a $\mu\mu$ pair with and an invariant mass in the range of the J/ψ or $\psi(2S)$. Alternately, by using a three muon trigger where a dimuon pair is present and satisfying the same mass criteria. All muon candidates satisfy ATLAS 'loose' criteria [4], and thresholds on muon momentum are adjusted depending on trigger and muon identification requirements.

Event with 4μ candidates and two opposite sign (OS) pairs have all their inner detector tracks fitted to a common vertex. Vertices of the two OS pairs (charmonium candidates) are refit with a J/ψ

or $\psi(2S)$ mass constraint [5]. Only events that satisfy the requirement of at least 1 reconstructed 4μ candidate are applicable, and with multiple candidates, the candidate with the lowest fit $\chi^2/ndof$ is selected. Background is reduced by restricting the fit quality using the $\chi^2/ndof$ measure, and limiting transverse distances between the primary vertex and the reconstructed 4μ vertex and the same primary vertex and the two di-μ sub-vertices. Signal and control regions are created by splitting below and above the di-charmonium separation in $\eta - \phi$ space, around $\Delta R = \sqrt{\Delta \eta^2 + \Delta \phi^2} = 0.25$, respectively. This split does not affect signal lineshape, but is used to validate the SPS shape and normalisation.

Improvements in the modelling of SPS and DPS backgrounds from the MC generation must be applied, kinematic corrections to this are derived from two dedicated control regions, and implemented using event weights on di-J/ψ p_T, $\Delta\phi$, and $\Delta\eta$. With these kinematic corrections, dedicated control regions for SPS and DPS are used to generate an estimate of their contribution. Additionally, non-prompt background is modelled using MC, control regions are created by inverting the vertex quality and transverse distance cuts. A summary of all cuts is shown in Table 1.

Signal region	Control region	Non-prompt region
Di-muon or tri-muon triggers, oppositely charged muons from each charmonium,		
loose muons, $p_T^{1,2,3,4} > 4, 4, 3, 3$ GeV and $|\eta_{1,2,3,4}| < 2.5$ for the four muons,		
$m_{J/\psi} \in [2.94, 3.25]$ GeV, or $m_{\psi(2S)} \in [3.56, 3.80]$ GeV,		
Loose vertex requirements $\chi^2_{4\mu}/N < 40$ ($N = 5$) and $\chi^2_{\text{di-}\mu}/N < 100$ ($N = 2$),		
Vertex $\chi^2_{4\mu}/N < 3$, $L_{xy}^{4\mu} < 0.2$ mm, $|L_{xy}^{\text{di-}\mu}| < 0.3$ mm, $m_{4\mu} < 11$ GeV,		Vertex $\chi^2_{4\mu}/N > 6$,
$\Delta R < 0.25$ between charmonia	$\Delta R \geq 0.25$ between charmonia	or $|L_{xy}^{\text{di-}\mu}| > 0.4$ mm

Table 1: Summary of cuts for each region

Single quarkonium and non-resonant di-μ events, are modelled using a data-driven approach as MC struggles to produce an accurate representation of this background. For this, create a control region for including fake muons, usually misidientified charged hadron tracks, by requiring that one of the charmonium candidates is reconstructed with a track from something other than a muon candidate. A transfer factor is derived from this area. For di-J/ψ, feeddown from the $J/\psi + \psi(2S)$ channel in the form of $\psi(2S) \to J/\psi + X$ decays are accounted for;

$$N_{fd} = \frac{\mathcal{B}'\epsilon'}{\mathcal{B}(\psi(2S) \to \mu\mu)\epsilon} N$$

$$B' = [B(\psi(2S) \to J/\psi + X) + B(\psi(2S) \to \gamma\chi_{cJ})B(\chi_{cJ} \to \gamma J/\psi)] \cdot B(J/\psi \to \mu\mu)$$

ϵ is efficiency, ϵ' for feeddown, N are yields, and $\mathcal{B}$ are branching fractions. B' is the branching fraction of the cascading feeddown;

4. Signal Modelling and likelihood fits

An unbinned maximum likelihood fit is used for the extraction of the signal in the 4μ mass spectrum with the likelihood function described in [6]. Background yields in the signal and control

regions are constrained together by a transfer factor which is obtained from the aforementioned background modelling. Two models are considered for each of the channels under examination. First, model the di-J/ψ channel with model A. The signal p.d.f. is built from the sum of three S-Wave Breight-Wiegner distributions that interfere, a phase space factor, and a convolution with a mass resolution function.

$$f_s(x) = \left[\sum_{i=0}^{2} \frac{z_i}{m_i^2 - x^2 - im_i\Gamma_i(x)} \right]^2 \sqrt{1 - \frac{4m_{J//\psi}^2}{x^2}} \otimes R(\theta)$$

A second Model B reduces this to two resonances, one non-interfering, and the other interacting with the SPS background, with p.d.f;

$$f(x) = \left[\frac{z_0}{m_0^2 - x^2 - im_0\Gamma_0(x)} + Ae^{i\phi} \right]^2 + \left[\frac{z_2}{m_w^2 - x^2 - im_2\Gamma_2(x)} \right]^2 \sqrt{1 - \frac{4m_{J//\psi}^2}{x^2}} \otimes R(\theta)$$

Here, A and ϕ define the SPS background amplitude and phase relative to m_0, the SPS Control region is removed from likelihoods. These models, Figure 1, are analogous to those in the LHCb study, though interferences between the signal resonances are in model A, unlike the LHCb work.
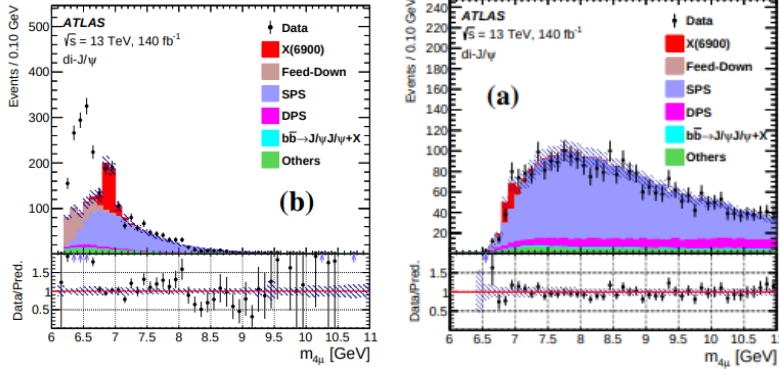
Figure 1: 4μ di-J/ψ mass spectrum in the signal and control regions before the fit.

To produce a likelihood model for the $J/\psi + \psi(2S)$ channel, Model α, introduce a 4th non-interfering resonance and assume the resonances also decay to $J/\psi + \psi(2S)$;

$$f_s(x) = \left(\left[\sum_{i=0}^{2} \frac{z_i}{m_i^2 - x^2 - im_i\Gamma_i(x)} \right]^2 + \left[\frac{z_3}{m_3^2 - x^2 - im_3\Gamma_3(x)} \right]^2 \right) \cdot \sqrt{1 - \frac{(m_{J//\psi} + m_{\psi(2S)})}{x^2}} \otimes R(\theta)$$

A final model β is built with a single resonance, corresponding to dropping the sum term in the α. Model α fixes the three masses in the interfering term to the values of the Model A fit leaving the final term to float 2.
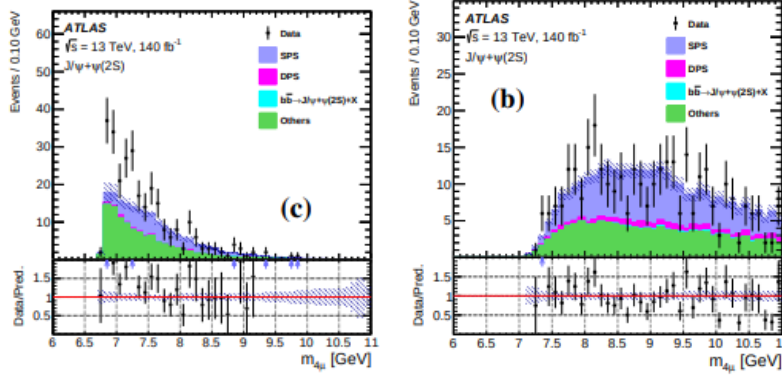
Figure 2: 4μ $J/\psi + \psi(2S)$ mass spectrum in the signal and control regions before the fit.

5. Results

Models A and B, Figure 3, both of these reproduce the data well. An excess of events above the background is observed here in the di-J/ψ channel. All resonances exhibit a significance of above 5 σ, including $X(6900)$. Significances are calculated by profile likelihood ratio.
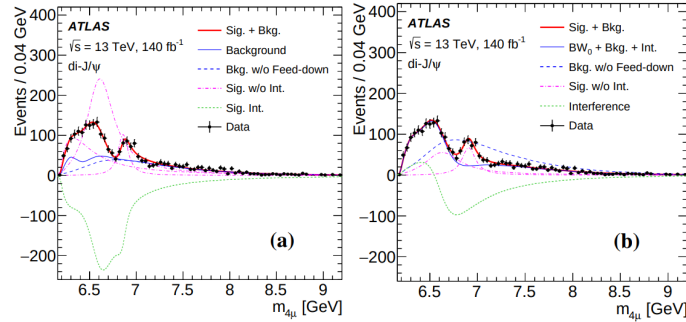
Figure 3: Fits of models A and B.

The broad structure at low mass could result from effects like feeddown from the higher di-Q resonances, like $T_{cc\bar{c}\bar{c}} \rightarrow \chi_{cJ}\chi_{cJ'} \rightarrow J/\psi J/\psi \gamma\gamma$. In the $J/\psi + \psi(2S)$ channel, Figure 4, signal significance with signal shape parameters of model α reaches 4.7 σ, and 4.3 σ for β. For α, the second resonance significance is 3.0 σ. The significance for all resonances and for the $X(6900)$ exceeds 5 σ, m_2 aligns with the LHCb mass. As is with the LHCb paper, a broad structure at lower mass and a resonance around 6.9 GeV are seen. All extracted values are shown in Table 2
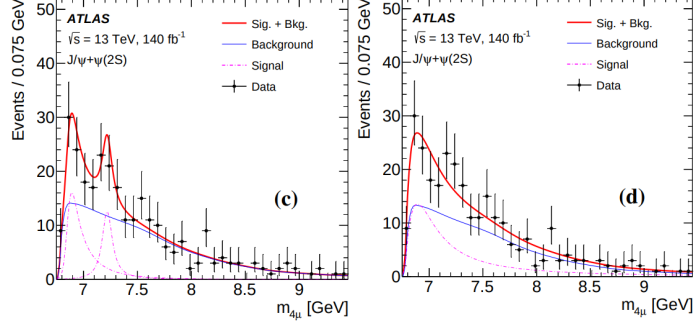
Figure 4: Fits of models α and β.

di-J/ψ	model A	model B
m_0	$6.41 \pm 0.08^{+0.08}_{-0.03}$	$6.65 \pm 0.02^{+0.03}_{-0.02}$
Γ_0	$0.59 \pm 0.35^{+0.12}_{-0.20}$	$0.44 \pm 0.05^{+0.06}_{-0.05}$
m_1	$6.63 \pm 0.05^{+0.08}_{-0.01}$	—
Γ_1	$0.35 \pm 0.11^{+0.11}_{-0.04}$	
m_2	$6.86 \pm 0.03^{+0.01}_{-0.02}$	$6.91 \pm 0.01 \pm 0.01$
Γ_2	$0.11 \pm 0.05^{+0.02}_{-0.01}$	$0.15 \pm 0.03 \pm 0.01$
$\Delta s/s$	$\pm 5.1\%^{+8.1\%}_{-8.9\%}$	—
$J/\psi + \psi(2S)$	model α	model β
m_3 or m	$7.22 \pm 0.03^{+0.01}_{-0.03}$	$6.96 \pm 0.05 \pm 0.03$
Γ_3 or Γ	$0.09 \pm 0.06^{+0.06}_{-0.03}$	$0.51 \pm 0.17^{+0.11}_{-0.10}$
$\Delta s/s$	$\pm 21\% \pm 14\%$	$\pm 20\% \pm 12\%$

Table 2: Extracted parameters.

6. Systematics

Only systematics producing an effect on the normalisations and the mass lineshape are considered, though only perturbations of the lineshape are of concern, signal and background normalisations are free-floating parameters. Sources of uncertainty here are the mass resolution, shape uncertainties, SPS modelling uncertainty, and residual mismodelling of the di-j/ψ p_T. Along with this, a number of fit changes are considered systematics, such as extra interferences and resonances, F-D wave Breight-Wiegner's, parameter biases, and more, Table 3

7. Conclusion

A search of a possible $cc\bar{c}\bar{c}$ state decaying into di$-J/\psi$ or a $J/\psi + \psi(2S)$ with $\sqrt{s} = 13$ TeV has been conducted [6]. With 140 fb^{-1} a large excess, of significance $> 5 \sigma$ in data is seen above background in the di-J/ψ channel, a broad structure at low mass is seen along with a resonance at 6.9 GeV. A three-resonance model with interferences and a model with the broader structure at

Systematic Uncertainties (MeV)	di-J/ψ		$J/\psi+\psi(2S)$	
	m_2	Γ_2	m_3	Γ_3
Muon calibration	±6	±7	<1	±1
SPS model parameter	±7	±7	<1	
SPS di-charmonium p_T	±7	±8	<1	
Background MC sample size	±7	±8	±1	<1
Mass resolution	±4	-3	-1	$^{+2}_{-4}$
Fit bias	-13	$+10$	$^{+9}_{-10}$	$^{+50}_{-16}$
Shape inconsistency	<1		±4	±6
Transfer factor	—		±5	±23
Presence of 4th resonance	<1		—	
Feed-down	$^{+4}_{-1}$	$^{+6}_{-2}$	—	
Interference of 4th resonance	—		-32	-11
P and D-wave BW	$+9$	$+19$	<1	±1
ΔR and muon p_T requirements	$^{+3}_{-2}$	$^{+6}_{-4}$	$^{+1}_{-2}$	-2

Table 3: Collected systematics.

lower $m_{4\mu}$ are more successful in describing the lineshape than cases with less or no interference. For the $J/\psi + \psi(2S)$ channel the excess is of the order 4.7 σ when using a two-resonance model, one near the 6.9 GeV threshold. The lower-mass structure cannot currently be discerned in detail; interpretations including non-interfering resonances, reflections and threshold enhancements cannot be discounted.

References

[1] Belle Collaboration *Observation of a narrow charmoniumlike state in exclusive $B^+ \to K^+ + \pi^+\pi^- J/\psi$ decays,* Physical Review Letters, 91(26), (2003).

[2] LHCb Collaboration *Observation of structure in the J/ψ-pair mass spectrum,* Science Bulletin 65 (2020) 1983, CERN, Geneva, (2020).

[3] M. A. Bedolla et al. *Spectrum of fully-heavy tetraquarks from a diquark+antidiquark perspective* Eur. Phys. J. C 80 (2020) 1004.

[4] ATLAS Collaboration *Muon reconstruction and identification efficiency in ATLAS using the full Run 2 pp collision data set at $\sqrt{s} = 13$ TeV,* Eur. Phys. J. C 81 (2021) 578

[5] P.A. Zyla et al. (Particle Data Group) *Review of Particle Physics,* PTEP 2020 (2020) 083C01 (cit. on pp. 6, 57).

[6] ATLAS Collaboration *Observation of an excess of di-charmonium events in the four-muon final state with the ATLAS Detector* Phys. Rev. Lett. 131 (2023) 151902.